A Hyperspectral Imaging System for In Vivo Optical Diagnostics

Hyperspectral Imaging Basic Principles, Instrumental Systems, and Applications of Biomedical Interest

BY TUAN VO-DINH, DAVID L. STOKES, MUSUNDI B. WABUYELE, MATT E. MARTIN, JOON MYONG SONG, RAMESH JAGANNATHAN, EDWARD MICHAUD, ROBERT J. LEE, AND XIAOGANG PAN

Optical techniques, often referred to as photonics, have recently had a dramatic effect on many different fields of research, including biomedical diagnostics [1]. Within this field, spectral imaging has been applied to the analysis of many different types of samples, ranging from individual biochemical species (e.g., NADH, tryptophan) observed in in vitro samples to organs of living people. These studies have given rise to new methods and instrumentation for the early or noninvasive diagnosis of various medical conditions, including arteriosclerosis, heart arrhythmia, cancer, and many other diseases. There is an especially strong interest in developing optical technologies that have the capability of performing in situ tissue diagnosis without the need for sample excision and processing. For example, fluorescence spectroscopy and imaging have been investigated for the diagnosis of almost every type of cancer and early neoplastic anomalies found in humans. The detection of early neoplastic changes is important from an outcome viewpoint, since, once invasive carcinoma and metastases have occurred, treatment is difficult. At present, excisional biopsy followed by histology is considered to be the "gold standard" for the diagnosis of early neoplastic changes and carcinoma. In some cases, cytology, rather than excisional biopsy, is performed. These techniques are powerful diagnostic tools because they provide high-resolution spatial and morphological information of the cellular and subcellular structures of tissues. The use of staining and processing can enhance visual contrast and specificity of histopathology. Both of these diagnostic procedures, however, require physical removal of specimens followed by tissue processing in a laboratory. These procedures incur a relatively high cost because specimen handling is required; more importantly, diagnostic information is not available in real time. Moreover, in the context of detecting early neoplastic changes, both excisional biopsy and cytology can have unacceptable false negative rates, often arising from sampling errors.

Optical techniques have the potential for performing in vivo diagnosis on tissue without the need for sample excision and processing. Another advantage of optical diagnosis is that the resulting information can be available in real time. In addition, since removal of tissue is not required for optical diagnosis, a more complete examination of the organ of interest can be achieved than with excisional biopsy or cytology. We have previously investigated the laser-induced fluorescence (LIF) technique for in vivo detection of gastro-intestinal cancer [2]–[4]. This LIF diagnostic information can be available in real time. In addition, since removal of tissue is not required for optical diagnostics, a more complete examination of the organ of interest can be achieved than with excisional biopsy or cytology. Another important application for optical diagnostic technologies is the possible use of these techniques for guidance during surgical intervention and treatment. In such surgical-assisted applications, the ability of optical diagnostic technologies to provide real-time information is critically useful.

Optical diagnostic technologies have been traditionally classified into two broad categories: spectroscopic diagnostics and optical imaging. Spectroscopic diagnostic techniques are generally used to obtain an entire spectrum of a single tissue site within a wavelength region of interest. These techniques are often referred to as point-measurement methods. On the other hand, optical imaging methods are aimed at recording a two-dimensional (2-D) image of an area of the sample of interest at one specific wavelength. A relatively new category, which combines the two modalities, is currently in an early development phase. This third category, often referred to hyperspectral imaging (HSI), is described in this article, which details the HSI basic principles and instrumental systems as well as its applications of biomedical interest.

The Principle of HSI

Figure 1 illustrates the HSI concept. HSI represents a hybrid modality for optical diagnostics, which obtains spectroscopic information and renders it in image form. With conventional spectroscopy, the signal at every wavelength within a spectral range can be recorded, but for only a single analyte spot. On the other hand, the HSI concept combines these two recording modalities and allows the recording of the entire emission for every pixel on the entire image in the field of view. The HSI approach provides a "data cube" of spectral information of the entire image at each wavelength of interest (Figure 2). Another approach, often referred to as

 0739-5175/04/$20.00©2004IEEE

multispectral imaging (MSI), involves recording optical images at only a few wavelengths (e.g., 2–5). MSI and HSI systems are different from the instrumental and data analysis point of views. Multispectral imaging systems often involve simple optical filter wheels and have been used previously in molecular luminescence [5], they have demonstrated the capability to acquire spatial and spectral information from numerous applications such as microscopy [6], multichannel analysis [7], and medicine [8]. HSI systems, conversely, were developed recently and use sophisticated tunable filters capable of recording images at a large number of wavelengths (20–100) with very narrow bandpasses.

The HSI system described in this article uses a rapid wavelength-scanning solid-state device, an acousto-optic tunable filter (AOTF), which operates as a tunable optical band pass filter. An AOTF offers the advantage of having no moving parts and can be scanned at very high rates (microsecond time scale). Since AOTFs with high spatial resolution and large optical apertures are available, they can be applied for spectral imaging applications [9]. The use of AOTFs for ultraviolet (UV)-visible, near infrared, and fluorescence spectroscopy has been reported [10]–[13]. Imaging fiber probes (IFP)-based coherent fiber optic bundles have been widely used in fiberscopes for endoscopic imaging applications. Here, we describe an HSI system combining a 2-D charge-coupled device (CCD) detector, an AOTF device, and optical imaging IFP technology.

The Operating Principle of AOTFs

Whereas MSI systems can use simple optical devices such as filter wheels that have several optical filters, HSI systems require continuously tunable filters having special types of dispersive devices capable of tuning to a large number of wavelengths in a short time period (microseconds to milliseconds). Tunable filters such as AOTFs and liquid crystal tunable filters (LCTFs), allow the investigator to rapidly record an image at various wavelengths. AOTFs are solid-state optical bandpass filters that can be tuned to various wavelengths within microseconds by varying the frequency of the acoustic wave propagating through the medium. The solid-state nature of an AOTF includes a high-throughput (90% diffraction efficiency) dispersive element with no moving parts, thus increasing the ruggedness of the instrumentation. AOTF devices consist of a piezoelectric transducer bonded to a birefringent crystal. The transducer is exited by a radio frequency (RF) (50–200 MHz) and generates acoustic waves in a birefringent crystal. These pressure waves establish a periodic modulation of the index of refraction of the crystal via the elasto-optic effect. As an applied acoustic wave propagates through the crystal, it creates a grating by alternately compressing and relaxing the lattice. Those density changes create periodic index of

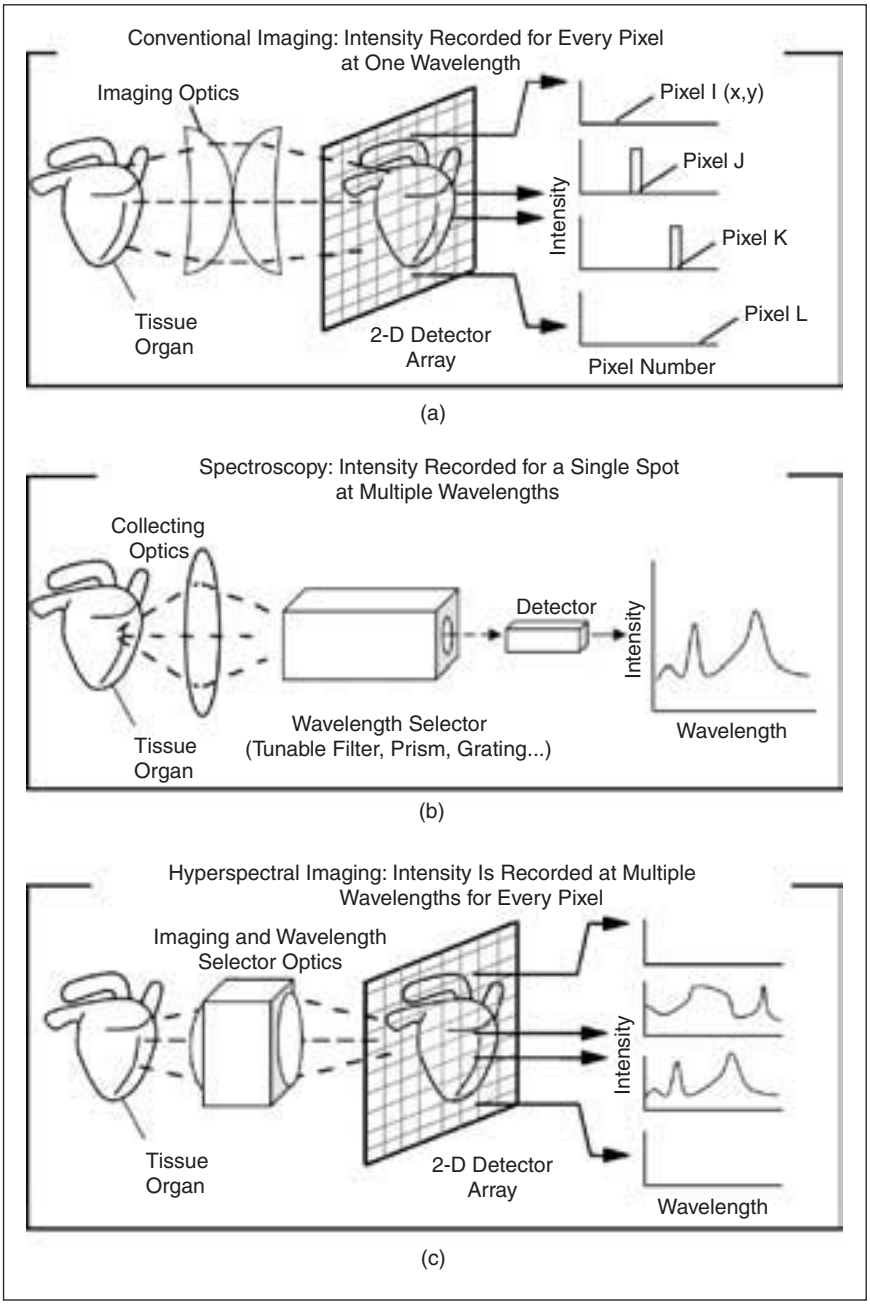

Fig. 1. Principle of HSI. (a) In conventional imaging, every pixel of an entire 2-D image can be recorded, but only at a specific wavelength or spectral bandpass; (b) in conventional spectroscopy, the optical spectrum at every wavelength within a spectral range can be recorded, but for only a single spot (or pixel); (c) the HSI concept combines these two recording modalities and allows recording the entire optical spectrum for every pixel on the entire 2-D image in the field of view.

Optical techniques have the potential for performing in vivo dignosis on tissue without the need for sample excision and processing.

refraction changes that act collectively like a transmission diffraction grating, except for the fact that only one wavelength is diffracted at a time. As a result, the AOTF behaves as a tunable filter. The wavelength of the diffracted beam is varied by changing the frequency of the acoustic wave, thereby also adjusting the grating spacing. This is the basis of an electronically tuned optical filter which operates via Bragg diffraction of light by periodic modulations in the index of refraction in the crystal established by the acoustic waves. The Bragg grating diffracts only light that enters the crystal within an angle normal to the face of the crystal. This range is called the acceptance angle of the AOTF. The percentage of light diffracted is the diffraction efficiency of the device. This parameter greatly depends on the incidence angle, the wavelength selected, and the power of the RF signal. For visible wavelengths in a tellurium oxide crystal (the diffraction medium of the AOTF), the applied acoustic wave is RF and can be switched very quickly (typically in less than 50 μs) compared to other technologies. Unlike an LCTF, where the bandwidth is fixed by the design and construction, an AOTF can vary the bandwidth by using closely spaced RF frequencies simultaneously.

In a typical AOTF, the first-order diffracted beam is separated from the undiffracted beam (i.e., the zero-order beam) by diffraction. The undiffracted beam exits the crystal at the same angle as the incident light beam, while the diffracted beam exits the AOTF at a small angle ($\sim$6°)with respect to the incident beam. A detector can be placed at a distance so that the diffracted light can be monitored, while the undiffracted light does not irradiate the detector. Figure 3 schematically illustrates the operating principle of a typical AOTF.

In addition, when the incident beam is linearly polarized and aligned with the crystal axis, the polarization of the diffracted beam is rotated 90° with respect to the undiffracted beam. This can provide a second means to separate the diffracted and undiffracted beams. One polarizer is placed before the AOTF and is aligned with the crystal. At the exit of the AOTF, a second polarizer is rotated 90° with respect to the first. The crossed polarizers block the undiffracted light, while most of the diffracted beam is transmitted through the AOTF crystal.

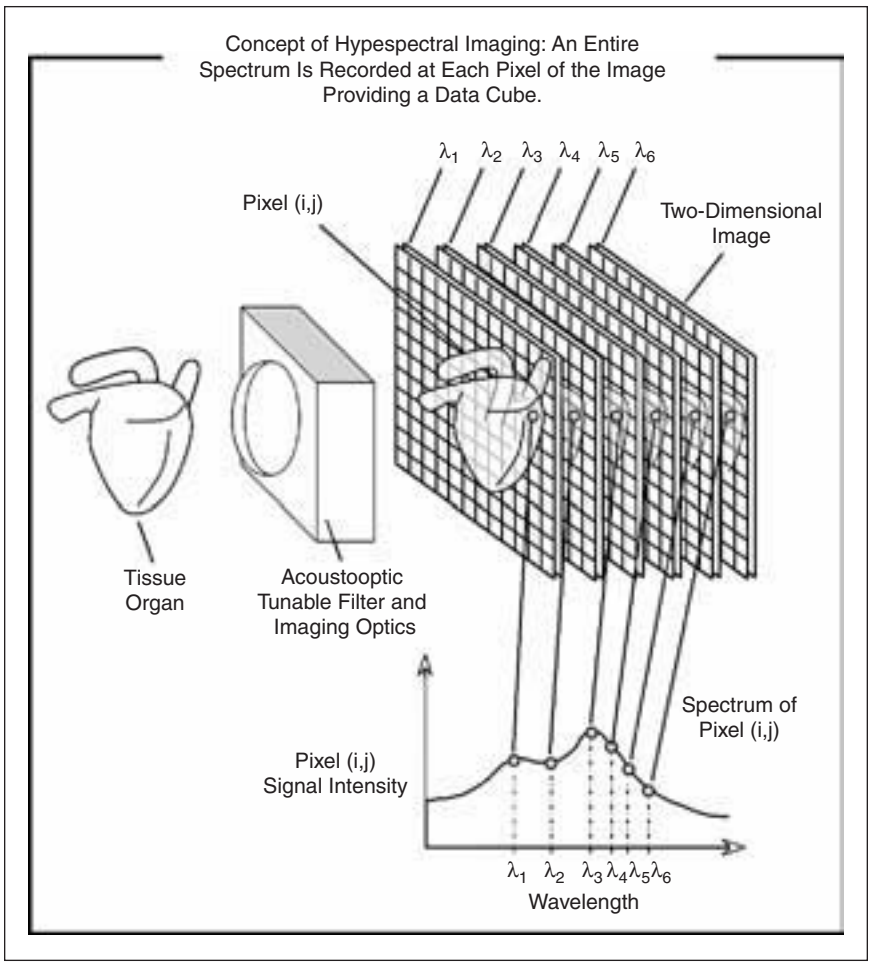

Fig. 2. Hyperspectral data cube. The HSI approach provides a "data cube" of spectral information, which consists of a series of optical images recorded at various wavelengths of interest.

HSI Systems and Materials

Two HSI systems were assembled for LIF-based imaging. One system was used for large viewing field areas and was applied to whole-specimen measurements. The second system employed an imaging optical fiber or an endoscope for small viewing field areas.

AOTF-based HSI Systems for Large Viewing Fields

The AOTF-based system is illustrated in Figure 4. An argon ion laser (Spectra Physics, Model Stabilite

HSI represents a hybrid modality for optical diagnostics, which obtains spectroscopic information and renders it in an image form.

2017) was the excitation source, providing 514.5-nm radiation. The laser beam was coupled to a fiberoptic bundle for transmission to the sample or organ of interest. A 2.5-cm (diameter) lens was used to project the laser beam from the laser onto the entrance end of the fiber bundle, slightly overfilling its aperture. The bundle was selected to provide a highly uniform excitation field on the sample. A 2.5-cm (diameter) lens with a focal length of 4 cm was used to collect the image and project it through an AOTF. The AOTF (Brimrose, Model TEAF5-0.3-1.3) projected the diffracted signal at an angle different from that of the nonselected radiation. The bandpass was approximately 2.5 nm. At a suitable distance beyond the AOTF, the nonselected radiation was spatially separated from the selected bandpass and could be rejected with a beam stop (iris diaphragm). In order to further reject out-of-band transmission, a pair of polarizers was used in crossed orientations. A holographic notch filter (Kaiser Optical Systems) was used to prevent any stray laser light from entering the imaging lens (Nikon, AF Micro Nikkor 105 mm) of the CCD. In the system evaluated, the CCD model ST-6, was purchased from Santa Barbara Instruments Group (SBIG). The operating spectral range was 330–900 nm. The detector was 8.63 × 6.53 mm and contained 375 × 242 pixels. Standard pixel size was 23 × 27 μm. Dark current could be kept as low as 13 electron/pixel/second at −20 °C. The detector was installed on a regulated thermo-electric Peltier effect-based cooler. Antiblooming protection was also included. The analog-to-digital resolution was 16 b. A mechanical shutter was included in the optical head to facilitate taking dark frames. The interface to the PC-compatible computer was accomplished via an RS232 system.

AOTF-Based Endoscopic HSI System for LIF Imaging

The imaging system based on an imaging optical fiber for remote, small-field monitoring is illustrated in Figure 5. An argon ion laser source was used to provide 514.5-nm excitation. An imaging fiber or an endoscope (Olympus, Model GIF Type 1T20) was modified to deliver excitation through the biopsy channel. In doing so, a 1-mm core optical fiber was fed through the biopsy channel to the endoscope probe head. Note that we used an endoscope in this work but any imaging fiber could also be used as the detection channel. To perform measurements inside organs such as the gastrointestinal tract, the endoscope provides a convenient detection channel for the MSI system. The laser beam was

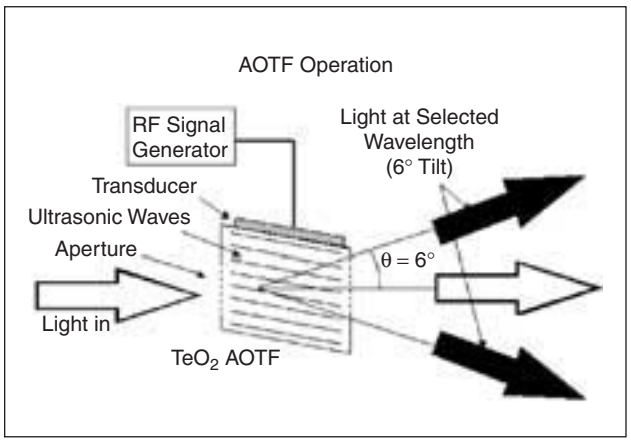

Fig. 3. Principle of operation of a typical AOTF. AOTF devices consist of a piezoelectric transducer bonded to a birefringent crystal. The transducer is excited by a radio frequency and generates acoustic waves in the birefringent crystal, creating a grating by alternately compressing and relaxing the lattice. Those density changes create periodic index of refraction changes that collectively act like a transmission diffraction grating. The first-order diffracted beam is separated from the undiffracted beam (i.e., zero-order beam); the undiffracted beam exits the crystal at the same angle as the incident light beam, while the diffracted beam exits the AOTF at a small angle with respect to the incident beam.

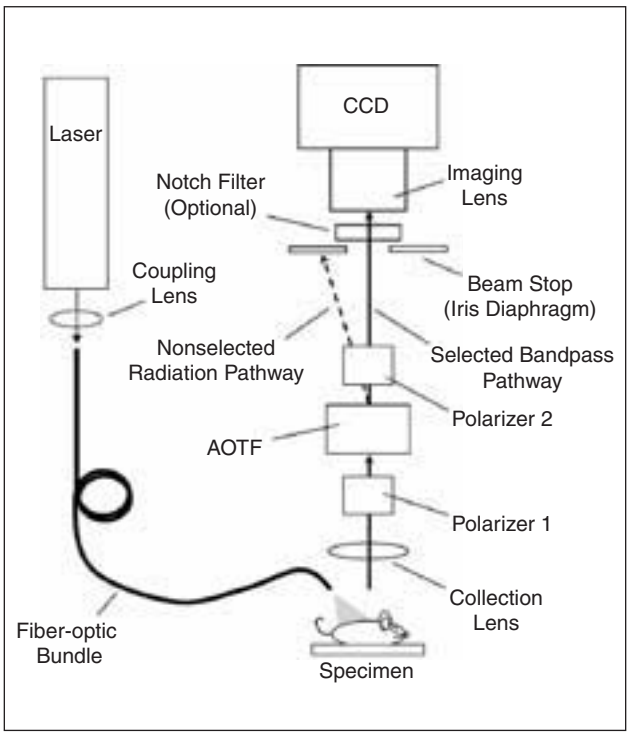

Fig. 4. A schematic diagram of an AOTF-based LIF imaging system for large viewing fields.

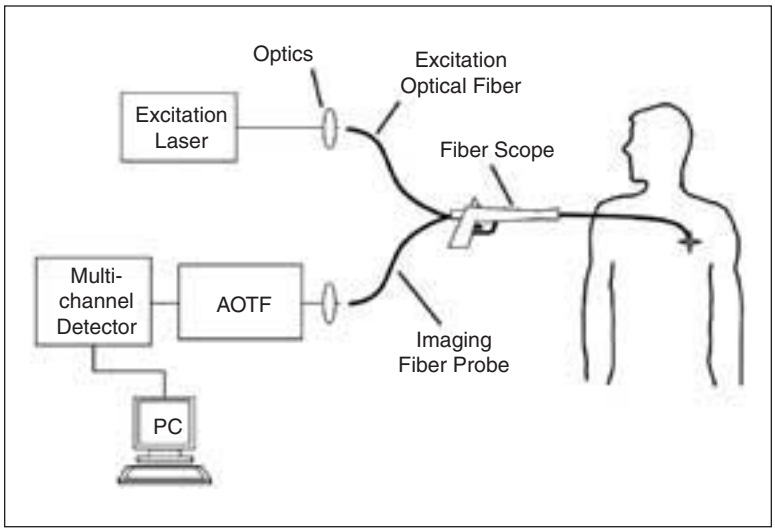

Fig. 5. An imaging system using an IFP inserted into an endoscope.

coupled to the excitation fiber via a conventional 2.5-cm f/1 lens for transmission to the probe head. The resulting LIF signal was collected by the imaging optical-fiber bundle of the endoscope and transmitted to the AOTF-based detection module. Within the detection module, the signal light was collimated with a 2.5-cm f/2.5 lens and projected through an AOTF (Brimrose, Model TEAF5-0.45-0.70). The bandpass was approximately 4 nm. As with the previous system, the selected bandpass was deflected from the original path of light propagation through the AOTF, and the nonselected radiation was spatially separated from the selected bandpass and rejected with a beam stop (iris diaphragm). A pair of cross-oriented polarizers was used to further reject out-of-band transmitted light.

The spectral resolution given by the manufacturer for the AOTF used in this study was 4 nm at 633 nm. The diffraction efficiency was relatively high, typically about 70% at 600 nm. The optical aperture was 10×10 mm, and the acceptance angle was greater than 30 °C. The drive power range was 1.0 to 1.5 W. The RF generator used (Brimrose-model AT) could apply 0–10 W of RF power and was controlled by a DOS-based computer using a 16-b computer controller board supplied by Brimrose. Custom software was developed at Oak Ridge National Laboratory to control the AOTF, supporting various scanning modes and fixed-frequency operation. In addition, a holographic notch filter (Kaiser Optical Systems) was used to prevent any stray laser light from entering the imaging lens (Nikon, AF Micro Nikon 105 mm) of the camera. The detector was an intensified CCD (ICCD) (Roper Scientific, Model PI-Max512-t18/G/II) operated at −20 °C The ICCD was controlled with Winspec software, provided by Roper Scientific.

Materials

The tissue samples (chicken brain and liver) were purchased from commercial meat suppliers in Knoxville, Tennessee. The mice studies were performed in accordance to the protocols approved by the Institutional Animal Care and Use Committee at Ohio State University and Oak Ridge National Laboratory. In this study we used three mice for evaluating the instrumental system. Male athymic BALB/c (nu/nu) mice weighing 18–22 g were purchased from Charles River Laboratories (Wilmington, Massachusetts). To generate a tumor xenograft, 10^6 kB human oral carcinoma cells were injected subcutaneously (s.c.) into a mouse using a 26-gauge needle in the upper chest area. The tumors reached palpable sizes of 10–20 mg in 14 days following tumor cell implantation and ∼400 mg at the time of the study (28 days post inoculation). To induce pPIX production, 10 mmoles/kg body weight of 5-aminolevulinic acid (5-ALA) was intraperitoneal (IP) injected in 100 μL of saline. Five minutes prior to spectral analyses and imaging, the mouse was anesthetized by IP injection of 100 mg/kg of ketamine and 10 mg/kg of xylazine dissolved in saline and secured on a board to allow easy visual access to the tumor. Additional IP injections of ketamine/xylazine were given as necessary to maintain unconsciousness of the mouse during the entire procedure. At the end of the study, the mouse was sacrificed via an overdose of the anesthetic.

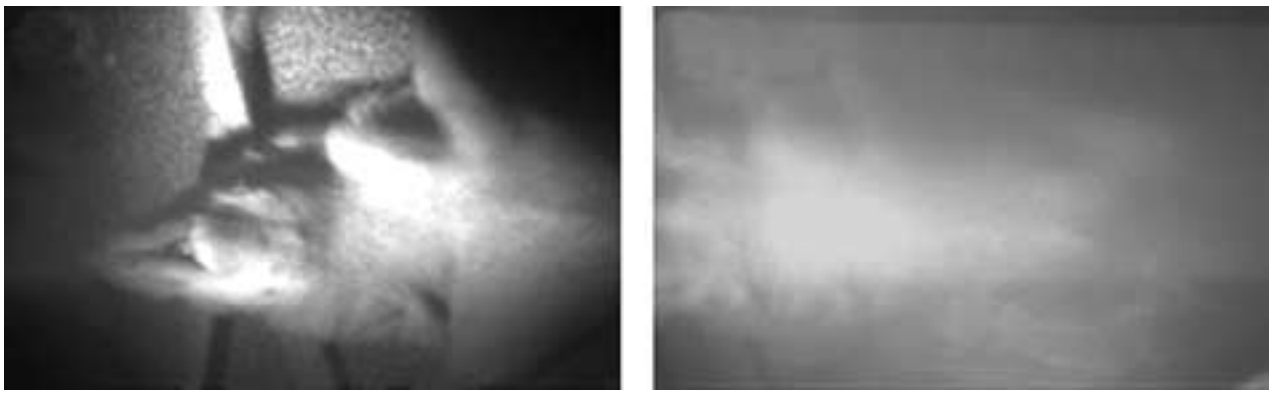

Fig. 6. A tumor-laden mouse large-field image acquired with an AOTF at (a) 514.5 nm and (b) 600 nm.

Results and Discussion

Large Field AOTF-based LIF Imaging System

In order to evaluate the optical quality of the newly assembled large field imaging system, images were recorded of tumor-laden, nude mice. Figure 6(a) shows a diffuse reflection image of a tumor-laden mouse, acquired with the AOTF bandpass tuned to 514.5 nm. The CCD exposure time was 0.1 s. The laser beam was projected onto the mouse, forming a 3.7-cm diameter excitation field. As depicted in the figure, the field of view included the ventral head and thorax region, with a tumor clearly visible in the right shoulder region. The highly resolved features of the mouth illustrate the optical quality of the AOTF based system. Figure 6(b) illustrates the same field of view, but with the AOTF tuned for 600-nm bandpass detection. The CCD exposure time was 0.25 s. Virtually no sharp-image reflection signal was detected at this wavelength; and, as illustrated by this image, no distinctive features from the mouse are resolved in this picture. The faint signal is a very weak and diffuse, possibly due to the background fluorescence from the mouse tissue. This result demonstrates the wavelength-discriminating power of the AOTF-based imaging system.

AOTF-Based Endoscope Imaging System

An endoscope was modified for LIF-based remote imaging of small viewing fields, with a long-term goal of gastrointestinal optical biopsy. For preliminary evaluations of system performance, several tissue samples were investigated as model systems. Figure 7(a) illustrates an LIF image of a thick section of sheep brain acquired with the endoscope. The image is an accumulation of 10 exposures of 5 s each. The excitation field was approximately 1.5-cm diameter with a laser power of approximately 500 mW. The sample was approximately 1.3 cm in diameter. In order to accentuate fluorescent features on the tissue, the sample was coated with a fluorescent dye solution (10^{-6} M Rhodamine 6-G). The AOTF was tuned to 560-nm, which corresponds to the LIF emission wavelength of the dye; the image shows strong fluorescence signal from fluorescent areas on the tissue. For comparison, Figure 7(b) shows an image of the same viewing field, with an AOTF setting of 514.5 nm, where no fluorescent image was expected. The wavelength discriminating power of the AOTF based system is clearly evident by the enhanced image of the tissue in the 560-nm image. Furthermore, optical quality is demonstrated in the 560-nm LIF image. Some minor features are resolved, including various dark spots throughout the tissue sample, measuring as small as 250-μm diameter.

The LIF imaging endoscope was also tested with a thin section of mouse kidney (Molecular Probes, F-24630). The section was labeled with three dyes: AlexaFluor 488 WGA, AlexaFluor 568 phalloidin, and DAPI. Regardless of the dyes, the thin tissue sample was virtually transparent to the naked eye in ambient light conditions. Figure 8(a) illustrates an LIF image of the kidney section, acquired with a bandpass of 560 nm. The excitation field parameters were the same as for the brain tissue images illustrated in Figure 7. The image is an accumulation of 10 exposures of 1 s each. The LIF detection capability dramatically enhances structural features of the kidney that would otherwise be difficult to see. For example, the inner boundary of the cortex region is clearly defined with slightly darker contrast with respect to the inner medulla region. The slender dark region in the right side of the sample is a cross section of the kidney pelvis, measuring approximately 0.4 cm in length. The

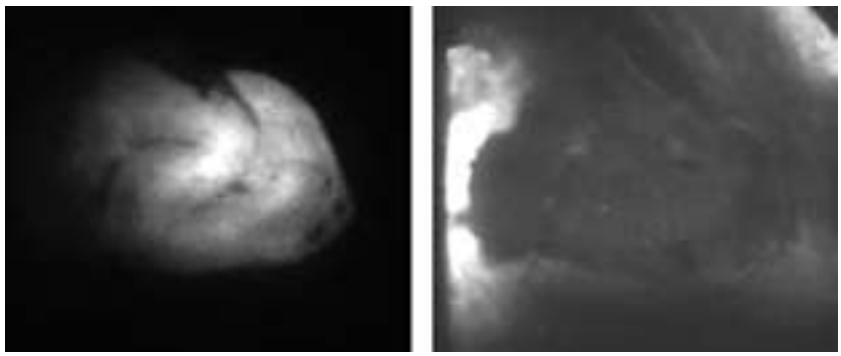

Fig. 7. Optical images of a section of sheep brain using an HSI system with the AOTF bandpass at (a) 560 nm and (b) 514.5 nm.

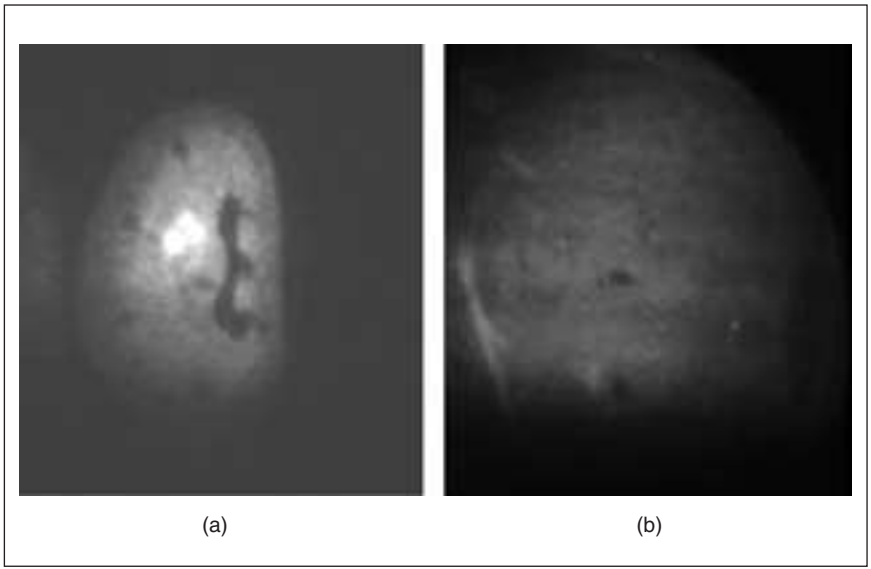

Fig. 8. Optical images of a section of mouse kidney using an HIS system with the AOTF bandpass at (a) 560 nm and (b) 514.5 nm.

HSI systems require continuously tunable filters having special types of dispersive devices capable of tuning to a large number of wavelengths in a short time period.

smaller, radial, dark features are cross section of calyces, measuring approximately 0.08 cm. In sharp contrast, Figure 8(b) illustrates an image of the same viewing field with a bandpass centered at 514.5 nm. At this wavelength, the thin kidney sample is virtually invisible. The faint glow exhibited by the image arises from reflection of the laser light from the sample platform. This background is clearly rejected in the image recorded at 560 nm, as shown in Figure 8(a).

Since a long-term application of the LIF-enhanced endoscope is its use in optical biopsy inside organs (including gastrointestinal and bronchial tracts), we have conducted measurements to evaluate the performance of the HIS instrument in collecting images of three-dimensional (3-D) model systems. In this study, we used a model of bronchial tubes (APM, Inc.) to evaluate the optical performance of the LIF-enhanced endoscope inside tubular tracts. The quality of both the excitation field and collected signal (e.g., uniformity, intensity, depth) are critical parameters in the performance of this system in these 3-D-sampling environments. Figure 9 shows LIF-based images acquired for various points in the bronchial tube model. Each image is an accumulation of 20 exposures of 1 s each. The laser power was approximately 500 mW. The AOTF bandpass was centered at 600 nm. The endoscope was inserted into the primary lumen. Figure 9(a) shows the first branch, with the lumen on each side of the branch leading to each lung. The endoscope probe head was positioned approximately 4 cm from the branch when acquiring the image. Ridges in the bronchial walls are clearly resolved in this picture. Furthermore, the depth of the image field in each of the major bronchial branched is evident. Figure 9(b) and (c) illustrates images more extensive bronchial branching acquired after the endoscope probe head was inserted further into the model. Figure 9(b) clearly demonstrates the 3-D imaging performance of the endoscope, as multiple lumen braches are observed at various distances directly in front the probe head. The lumen diameters in this picture range from 0.75 to 1.5 cm. The 3-D imaging power and LIF-enhanced contrast of the endoscope also enables detection of branches not occurring directly in line with probe head. For example, Figure 9(c) illustrates the lumen of two branches in a bronchial tube wall, each with propagation nearly perpendicular to the optical axis of the endoscope probe head.

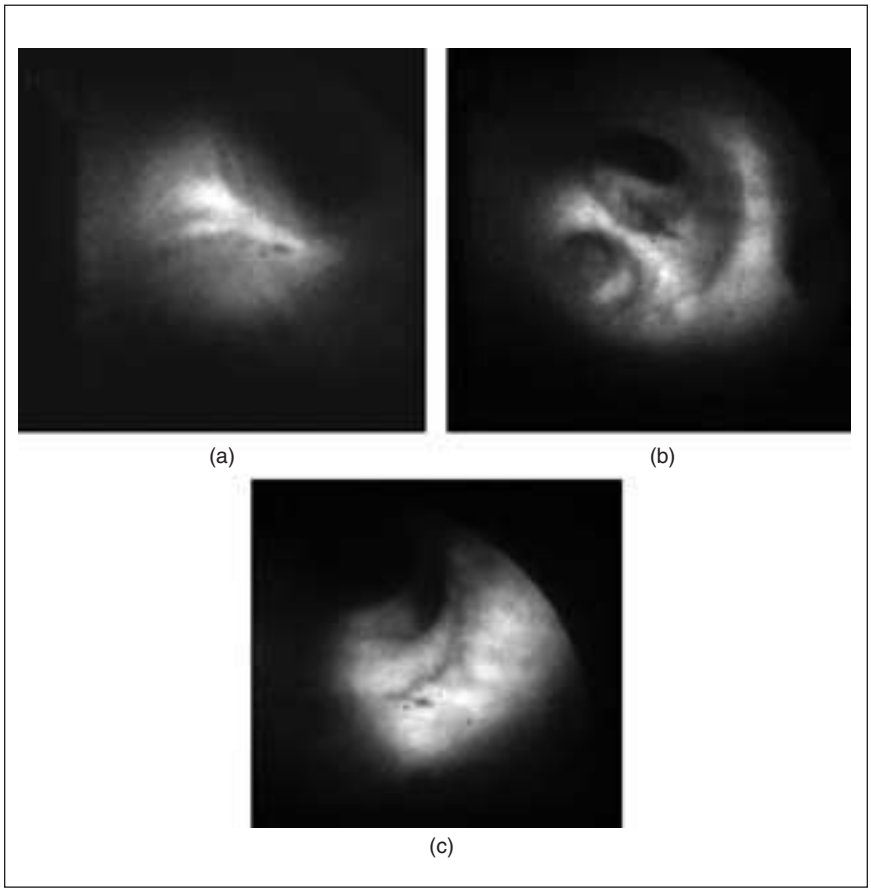

Fig. 9. Endoscopic LIF images of lumen sections of a bronchial tube model an HSI system with the AOTF bandpass at 600 nm.

HSI of Chicken Liver Tissue Fluorescence

Another application of HSI is well illustrated in the case of fluorescence images obtained on chicken liver samples. Figure 10(a) shows the autofluorescence images collected while scanning the AOTF of the HIS system within the wavelength range between 573–695 nm. These HSI fluorescence images depicted in a data cube format are shown in Figure 10(b). In this study, the excitation source was an Argon-ion laser emission line at 457 nm. The results indicated that autofluorescence images, having AOTF scanned in the region between 623–634 nm showed highly intense fluorescent spots (referred to as active spots). As

the AOTF was scanned beyond 645.9 nm, a decrease in the fluorescence of a given active spot in the tissue sample was observed. AOTF scanning in the wavelength range 490–564 nm did not show any significant tissue fluorescence (data not shown). Fluorescence images collected on a different spot (outside the active spots) in the same liver tissue sample did not exhibit fluorescence. Figure 11 shows the variation of the fluorescence intensity for two different spots in the chicken liver sample, viz., a strongly fluorescent spot (i.e., active spot) and a nonfluorescent spot. The fluorescence intensity of the active spot increased from 600 nm and reached maximum at 634.5 nm. The fluorescence intensity decreased as the AOTF scanning progressed to 700 nm. In contrast, the nonfluorescence spot exhibited no fluorescence over the entire AOTF scanning region (490–700 nm). The fluorescence obtained on the active spot in liver tissue was due to concentrated regions of porphyrin, which is the characteristic biomarker of liver tissue. Porphyrin compounds have characteristic fluorescence emission with a maximum around 630 nm. It is well known that the liver is an active site for the biosynthesis of heme and porphyrin-related biomarkers, which are intermediates of heme biosynthetic pathway [14]. This could explain our results where specific sites on the liver tissue showed intense fluorescence characteristic of porphyrins. The results of this study illustrate the usefulness of the HSI device in optical diagnostics. Our previous studies using point-detection LIF methods have demonstrated that autofluorescence properties of tissue can be exploited in the diagnosis of esophagus cancer [2]–[4] and of skin cancer [15]. It is known that changes in the content of NADH, collagen and porphyrin-related compounds can be used to differentiate normal and malignant lesions using LIF [16]. The AOTF-based HSI system provides the technological advantage in collecting biomarker specific autofluorescence of the 2-D image of an organ, enhancing data collection efficiency, particularly in the case of cancer diagnosis. In addition, the HSI system will have potential application in photodiagnosis of malignancy where porphyrins and derivatives are accumulated in malignant cells compared to the controls [17].

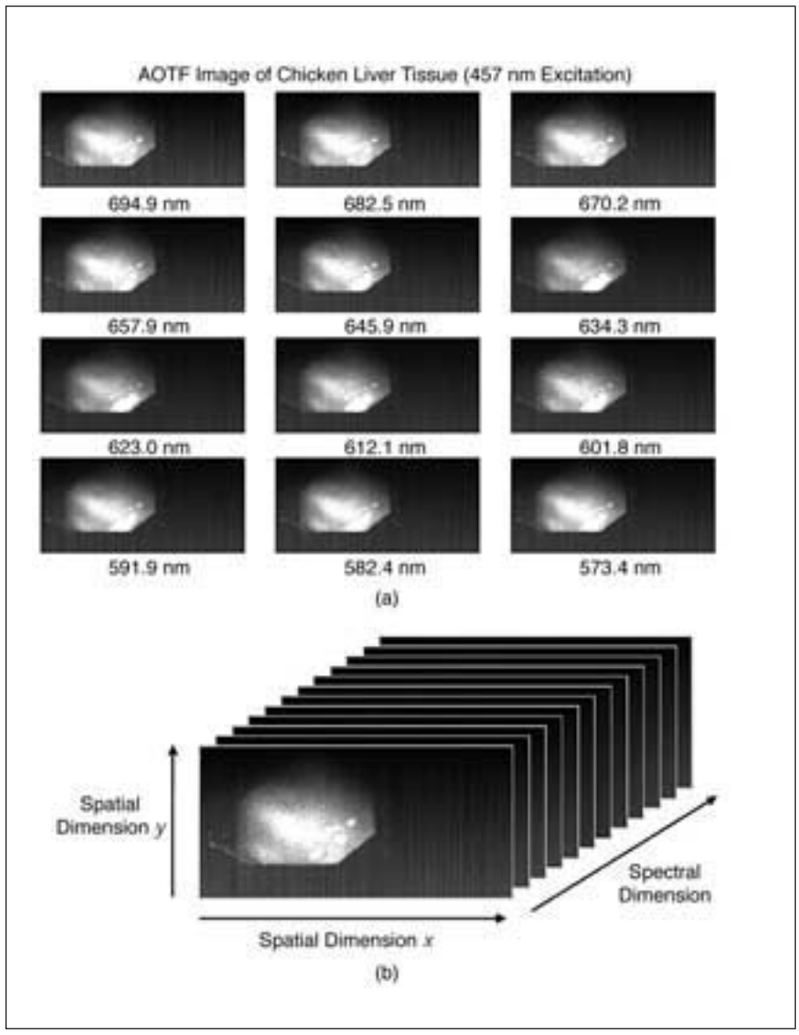

Fig. 10. (a) Fluorescence images of chicken liver collected at various wavelengths using the HSI system. (b) an HSI data cube of chicken liver fluorescence images.

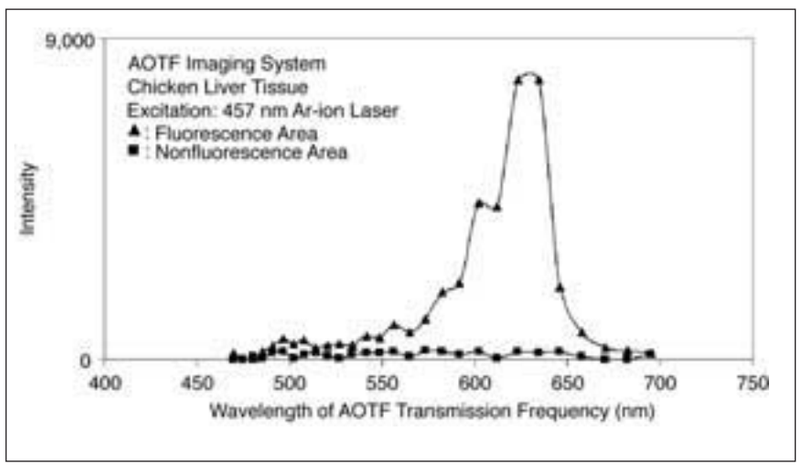

Fig. 11. Fluorescence spectra for two different sites on chicken liver sample (a strongly fluorescent spot and a nonfluorescent spot).

Conclusion

We have described the development of an HSI system that combines recent advances in several photonic technologies, including an AOTF, a 2-D CCD detector, and imaging fiberoptics. The integration of these technologies leads to a versatile and powerful imaging system that can rapidly record spectral images of samples at a series of wavelengths of interest. This imaging system could find useful applications in medical diagnostic applications where rapid in vivo detection of complex samples is required. The HSI technique has the potential for in situ diagnosis on tissue without the need for sample excision and processing. This diagnostic information can be available in real time. In addition, since the removal of tissue is not required for optical diagnostics, a more complete 2-D examination of the organ of interest can be achieved than with excisional biopsy or cytology. Another important application for optical HSI technologies is the possible use of these techniques for guidance of surgical intervention and treatment. In such surgical-assist applications, the ability of optical diagnostic technologies to provide real-time information is critically useful. The optical diagnostic approaches may either be an imaging modality or a spectroscopic modality. In either case, but especially with the imaging modality, one can provide more precise guidance of surgical intervention. The spectroscopic diagnostics may also be used to provide real-time assessment of tissue response to therapy.

Acknowledgments

This work was sponsored by the National Institutes of Health (Grant RO1 CA88787-01) and by the Office of Biological and Environmental Research, Department of Energy, under Contract DEAC05-00OR22725 with UT-Battelle, LLC. This research was also supported in part by the appointment of D.L. Stokes, J.M. Song, and R. Jagannathan to the U.S. Department of Energy Laboratory Cooperative Postdoctoral Research Training Program administered by Oak Ridge Institute of Science and Education.

Tuan Vo-Dinh is a corporate fellow at Oak Ridge National Laboratory (ORNL), Oak Ridge, Tennessee; group leader of ORNL's Advanced Biomedical Science and Technology Group; and the director of the Center for Advanced Biomedical Photonics at ORNL. His research has focused on the development of advanced technologies for the protection of the environment and the improvement of human health. His research activities involve laser spectroscopy, molecular imaging, medical diagnostics, cancer detection, chemical sensors, biosensors, nanosensors, and biochips. Dr. Vo-Dinh has published over 300 peer-reviewed scientific papers, is an author of a textbook on spectroscopy, and is the editor of four books. He holds over 28 patents, five of which have been licensed to environmental and biotech companies for commercial development. Dr. Vo-Dinh is a fellow of the American Institute of Chemists and a fellow of SPIE, the International Society for Optical Engineering, and a fellow of the American Institute for Medical and Biological Engineering. Dr. Vo-Dinh has received numerous awards including seven R&D 100 Awards for Most Technologically Significant Advance in Research and Development for his pioneering research and inventions of innovative technologies. In 1997, Dr. Vo-Dinh was presented the Exceptional Services Award for distinguished contribution to a Healthy Citizenry from the U.S. Department of Energy.

David L. Stokes received his Ph.D. in Chemistry from the University of Tennessee in 1999, and his B.S. in Physics (broad science) from the University of the South, Sewanee, in 1988. From 1988–2003, Dr. Stokes performed analytical chemistry research at Oak Ridge National Laboratory. His expertise spans many areas of molecular spectroscopy, with applications in remote sensors for environmental and biomedical studies. He is currently employed by EOIR Technologies, Woodbridge, Virginia, where he works as a sensors research scientist.

Musundi B. Wabuyele is currently a postdoctoral research associate with Dr. Tuan Vo-Dinh at Oak Ridge National Laboratory, Oak Ridge, Tennessee. He graduated with a B.S. in chemistry in December, 1997 from the University of Nairobi. He received his Ph.D. in analytical chemistry from Louisiana State University in May 2003. During his graduate work, he worked on the development of novel diagnostic assays that utilize single molecule detection techniques in polymer-based microfluidic devices to analyze biological molecules including DNA and proteins. His current research areas include biomedical imaging, nanotechnology and biosensors.

Matt E. Martin received the B.S. in mechanical engineering degree from Tennessee Technological University, Cookeville, Tennessee, in 1998, and the M.S.M.E. degree from Tennessee Technological University in 2000. His thesis topic was "Microscopic Thermal Detector Optimization through Material and Geometric Selection." He then went to work for Haleos, Inc., a start-up firm that designed and built novel fiber optic subcomponents and MEMS devices. He is currently pursuing a Ph.D. degree in mechanical engineering from Tennessee Technological University and is performing his research at Oak Ridge National Laboratory. Matt's current research topics include MEMS biosensor development, laser-induced fluorescence, and chemical detection using Raman scattering.

Joon Myong Song received his B.S. in chemistry from Sogang University in South Korea in 1991 and his Ph.D. degree in molecular science and technology from Kyushu University in Japan in 1997. In 2004, he joined the faculty at Chungnam National University in South Korea, where he is currently an assistant professor in the Department of Chemistry. His research interests include methods and applications of biosensors and micorfluidics based on spectroscopic methods for in vivo and in vitro biomedical study. He has written over 20 peer-review publications and over 20 proceedings and meeting abstracts.

Ramesh Jagannathan received his Ph.D. degree in biophysics from Indian Institute of Science, Bangalore, India. Since 2002, he has been working as a post-doctoral fellow in the Life sciences Division, Oak Ridge National Laboratory. His main interests are in the area of biomolecular and biomedical science and technology applied to cancer diagnosis and therapy, neurodegenerative disorders and infectious diseases.

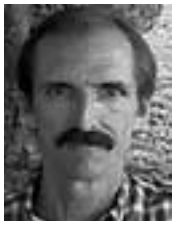

Edward Michaud is a senior staff scientist in the Mammalian Genetics and Genomics group at the Oak Ridge National Laboratory (ORNL). He received a B.S. from the University of Central Florida in 1979, an M.S. from Texas A&M University in 1984, and a Ph.D. from the University of Tennessee, Knoxville, in 1990. Dr. Michaud was an Alexander Hollaender Distinguished Postdoctoral Fellow in the laboratory of Dr. Richard Woychik at ORNL from 1991–1995, and, in 1996, he joined the staff at ORNL. Dr. Michaud's research interests are in using the tools of mouse genetics and functional genomics for determining the biological functions of human genes, with an emphasis on skin biology and cancer.

Robert J. Lee is an associate professor of pharmaceutics in The Ohio State University (OSU) College of Pharmacy and Comprehensive Cancer Center. He received his Ph.D. degree in 1994 from the Purdue University Department of Chemistry and postdoctoral training at the University of Pittsburgh Medical School Department of Pharmacology. He has since worked in the biotech industry in Gene Medicine Inc. and Endocyte Inc. before joining the faculty of OSU in 1997. Research in Dr. Lee's lab is focused on the development of tumor-targeted delivery systems for imaging and therapeutic systems, including the development of receptor targeted agents and lipid nanoparticles for optical imaging and photodynamic therapy.

Xiaogang Pan is currently a Ph.D. student in the research group of Dr. Robert Lee in The Ohio State University (OSU) College of Pharmacy. He received his bachelor degree in chemical pharmaceuticals from East China University of Science and Technology in 1996. He has worked in Shanghai Pharmaceutical Industry Design Institute from 1996–2000. His research is focused on the development of tumor-targeted delivery systems for imaging and therapeutic systems.

Address for Correspondence: Tuan Vo-Dinh, Center for Advanced Biomedical Photonics, Life Sciences Division, Oak Ridge National Laboratory, Oak Ridge, TN 37831-6101 USA. E-mail: vodinht@ornl.gov.

References

[1] T. Vo-Dinh, Ed., *Biomedical Photonics Handbook*, Boca Raton, FL: CRC, 2003.
[2] T. Vo-Dinh, M. Panjehpour, B.D. Overholt, C. Farris, and R. Sneed, "In vivo cancer diagnosis of the esophagus using differential normalized fluorescence (DNF) indices," *Laser in Surgery and Medicine*, vol. 16, pp. 41–47, 1995.
[3] M. Panjehpour, B.F. Overholt, T. Vo-Dinh, C. Farris, R. Sneed, and P. Buckley, "Spectroscopic diagnosis of esophageal cancer: New classification model, improved measurement system," *Gastrointestinal Endosc.*, vol. 41, pp. 577–581, 1995.
[4] T. Vo-Dinh, M. Panjehpour, B.F. Overholt, and P. Buckley, III, "Laser-induced differential fluorescence for cancer diagnosis without biopsy," *Appl. Spectrosc.*, vol. 51, pp. 58–63, 1997.
[5] G.H. Gao and Z. Lin, "Acoustooptic super multispectral imaging," *Appl. Opt.*, vol. 32, pp. 3081–3086, 1993.
[6] P.M. Delaney, M.R. Harris, and R.G. King, "Fiberoptic laser-scanning confocal microscope suitable for fluorescence imaging," *Appl. Opt.*, vol. 33, pp. 573–577, 1994.
[7] C.A. Bunting, P.G. Carolan, M.J. Forrest, P.G. Noonan, and A.C. Sharpe, "CCD camera as a multichannel analyzer for the spectral and azimuthal resolution of Fabry-Perot fringes," *Rev. Sci. Instr.*, vol. 59, 1488–1490, 1988.
[8] S.J. Andersson-Engels, J. Johansson, K. Svanberg, and S. Svanberg, "Fluorescence imaging and point measurement of tissue: Applications to the demarcation of malignant tumors and artheoscleotic lesions from normal tissue," *Photochem. Photobiol.*, vol. 53, pp. 807–812, 1991.
[9] L.J. Cheng, T.H. Chao, M. Dowdy, C.C. LaBaw, J.C. Mahoney, G.F. Reyes, and K. Bergman, "Multispectral imaging systems using acousto-optic tunable filter," *Proc. SPIE*, vol. 1874, pp. 224–231, 1993.
[10] P.J. Treado, I.W. Levin, and E.N. Lewis, "High-fidelity Raman imaging spectrometry—A rapid method using an acoustooptic tunable filter," *Appl. Spectrosc.*, vol. 46, pp. 1211–1216, 1992.
[11] I.C. Chang, "Acoustooptic tunable filters," *Opt. Eng.*, vol. 20, pp. 824–829, 1981.
[12] C.D. Tran and R.J. Furlan, "Electronic tuning, amplitude-modulation of lasers by a computer-controlled acoustooptic tunable filter," *Appl. Spectrosc.*, vol. 46, pp. 1092–1095, 1992.
[13] B. Cullum, J. Mobley, Z. Chi, D.L. Stokes, G.H. Miller, and T. Vo-Dinh, "Development of a compact, handheld Raman instrument with no moving parts for use in field analysis," *Rev. Sci. Instrum.*, vol. 71, pp. 1602–1607, 2000.
[14] J.R. Bloomer, "Liver metabolism of porphyrins and heme," *J. Gastroenterol. Hepatol*, vol. 13, pp. 324–329, 1998.
[15] M. Panjehpour, J. Clarke, M. Phan, T. Vo-Dinh, and S. Overholt, "Laser-induced fluorescence spectroscopy for in vivo diagnosis of non-melanoma skin cancers," *Laser in Surgery and Medicine*, vol. 31, pp. 367–373, 2002.
[16] S.P. Schantz, H.E. Savage, P. Sacks, and R.R. Alfano, "Native cellular fluorescence and its application to cancer prevention," *Environ. Health. Persp.*, vol. 105, pp. 941–944, 1997.
[17] C.J. Kelty, N.J. Brown, M.W. Reed, and R. Ackroyd, "The use of 5-aminolaevulinic acid as a photosensitiser in photodynamic therapy and photodiagnosis," *Photochem. Photobiol. Sci.*, vol. 1, pp. 158–168, 2002.